Silicon photonic crystal microarrays for high throughput label-free detection of lung cancer cell line lysates with sensitivity and specificity

Swapnajit Chakravarty[a], Wei-Cheng Lai[b], Yi Zou[b], Robert M. Gemmill[c], Ray T. Chen*[a,b],
[a]Omega Optics Inc., 10306 Sausalito Drive, Austin, TX, USA 78759; [b]Dept. of Electrical and Computer Engineering, University of Texas, 10100 Burnet Road Bldg. 160, Austin, TX USA 78758;
[c]Medical University of South Carolina, 96 Jonathan Lucas Street, Charleston, SC 29425;

ABSTRACT

Detection of biomolecules on microarrays based on label-free on-chip optical biosensors is very attractive since this format avoids complex chemistries caused by steric hindrance of labels. Application areas include the detection of cancers and allergens, and food-borne pathogens to name a few. We have demonstrated photonic crystal microcavity biosensors with high sensitivity down to 1pM concentrations (67pg/ml). High sensitivities were achieved by slow light engineering which reduced the radiation loss and increased the stored energy in the photonic crystal microcavity resonance mode. Resonances with high quality factor Q~26,760 in liquid ambient, coupled with larger optical mode volumes allowed enhanced interaction with the analyte biomolecules which resulted in sensitivities down to 10 cells per micro-liter to lung cancer cell lysates. The specificity of detection was ensured by multiplexed detections from multiple photonic crystal microcavities arrayed on the arms of a multimode interference power splitter. Specific binding interactions and control experiments were performed simultaneously at the same instant of time with the same 60 micro-liter sample volume. Specificity is further ensured by sandwich assay methods in the multiplexed experiment. Sandwich assay based amplification increased the sensitivity further resulting in the detection of lung cancer cell lysates down to concentrations of 2 cells per micro-liter. The miniaturization enabled by photonic crystal biosensors coupled with waveguide interconnected layout thus offers the potential of high throughput proteomics with high sensitivity and specificity.

Keywords: photonic crystal waveguide, photonic crystal microarray, biosensor, lung cancer detection, multiplexed assay, label-free, high throughput.

1. INTRODUCTION

Biomolecule detection by microarrays based upon label-free on-chip optical biosensors [1-4] is very attractive since this format avoids complex chemistries caused by steric hindrance of labels. Furthermore, chip-integrated technologies allow miniaturization towards the ultimate goal of personalized diagnostic assays for detecting toxins, allergens or biomarkers of disease, including cancer. Surface plasmon resonance (SPR) biosensors by Biacore [3], and the Biomolecular Interaction Detector (BIND) platform [4] based on one-dimensional gratings in polymer substrates represent two technologies that have achieved commercial success. Recently, Genalyte has started commercializing ring resonator based silicon micro-photonic devices for label-free microarrays [1]. However, high sensitivities from nanophotonic devices promise still better sensitivity and miniaturization.

Devices based on two-dimensional nano-photonic crystals (PCs) in silicon [5-9], have demonstrated the ability to confine and guide slow light on length scales of the wavelength of light. High sensitivity and miniaturization into compact sensors have been demonstrated for chemical [10] and bio-sensing [5-9]. Yet, concerns remain regarding the specificity of the label-free interaction that is detected. Specificity can be statistically determined from the results of multiple sensor spots and also by using sandwich assay techniques. We recently showed that high sensitivity PC microcavity sensors can be multiplexed on a chip and measured simultaneously in a single measurement. Using interconnecting on-chip waveguides, redundant measurements in multiple locations can be performed at the same instant of time [11]. In this paper we review various design aspects that have enabled high sensitivity demonstration of photonic crystal microarrays culminating in the first demonstration of multiplexed sandwich assay detection using the PC biosensor platform, combining simultaneous specific and control binding experiments for the detection of a biomarker from lung cancer cell lysates.

*raychen@uts.cc.utexas.edu; phone 1 512-471-7035; fax 1 512-471-8575; bart.mer.utexas.edu:16080/Chen/optic-inter/
Frontiers in Biological Detection: From Nanosensors to Systems V, edited by
Benjamin L. Miller, Philippe M. Fauchet, Proc. of SPIE Vol. 8570, 857005

2. SENSING PRINCIPLE

The device consists of a triangular lattice of air holes etched into silicon in a silicon-on-insulator (SOI) substrate. Photonic crystal (PC) waveguides are defined and photonic crystal microcavities are fabricated along the photonic crystal waveguide (PCW). The resonant wavelength of a PC microcavity is dependent on the geometry of the microcavity. Light propagating in the PCW couples to a PC microcavity at the resonant wavelength of the PC microcavity. The transmission spectrum of the PCWs consequently show minima corresponding to the resonant wavelength of the PC microcavity. Probe proteins for bio-agents and pathogens, each specific to a unique target molecule for diagnostic distinction, are patterned on a unique microcavity using ink-jet printing while preserving protein functionality. When a target molecule binds with its specific probe, the resonant wavelength of that microcavity shifts which consequently shifts the corresponding minimum in the waveguide transmission spectrum. The shift in the minimum in the transmission spectrum identifies the occurrence of a binding event. The magnitude of binding is determined by De Feijter's formula [12] that relates the absolute amount of adsorbed molecules M with the change in refractive index as:

$$M = d_A \frac{n_A - n_C}{dn/dc}$$

where d_A is the thickness of adsorbed layer, n_A is the refractive index of adsorbed molecules, n_C is the refractive index of cover solution and dn/dc is the change in refractive index of molecules which is proportional to the shift $d\lambda$ in position of the resonance peak [13]. The magnitude of resonant wavelength shift is proportional to the amount of adsorbed biomolecules and hence provides a label-free means to quantitatively determine biomolecules of interest.

3. DEVICE DESIGN

A quick literature survey shows that research groups have used different biomolecule conjugates of target receptor biomolecules and probe biomolecules, for sensing experiments. Sensitivity comparisons have been made based on the minimum mass sensing capabilities of different sensing platforms [14]. However, binding kinetics between the target receptor biomolecules and probe biomolecules in solution, also determines the sensitivity of photonic crystal biosensors. In addition, the focus of nanophotonics research has been primarily to develop the smallest sensor. Researchers have thus tried to balance two contradictory requirements of sensitivity and quality factor. However, attempts to reduce the resonator size or increase the optical mode overlap with the analyte leads to a reduction in resonance quality factor and hence the ability of the device to detect small concentrations as well as small changes in concentration. One aspect that is overlooked in such hybrid biosensors for microarray applications is that the individual sensors in the array must be functionalized with unique receptor/capture biomolecules.

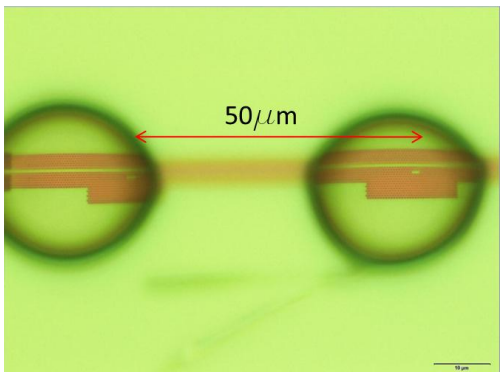

Fig. 1: Ink-jet printed spots on two adjacent photonic crystal microcavities. The scale bar is for 10μm.

When the resonators are patterned via ink-jet printing or microfluidic channels, the receptor/capture biomolecules are actually dispensed over a significantly larger area. A microscope image of a patterned device with an array of two PC microcavities is shown in Fig. 1. In Fig. 1, we note that by ink-jet patterning, the minimum dispensed spot size of biomolecules is ~35μm. The ink-jet dispensed spot size determines the minimum spacing between adjacent sensors, and is different from the device surface area that can be functionalized by combining lithographic patterning with ink-jet printing [15]. Hence, from practical considerations, there is room to achieve both requirements of sensitivity and high Q

by engineering designs that are slightly larger than conventional approaches. We show that deviating from current trends and slightly increasing the sizes of photonic crystal microcavities can enhance the resonance Q and at the same time, enhance the optical mode overlap with the analyte, thereby leading to the highest sensitivity as we have demonstrated for different dissociation constants. [8, 16] The optimum design requires an understanding of the sources of loss in a PC microcavity and design methods to overcome the losses in a robust device structure.

The total quality factor Q_T of the resonance mode of a PC microcavity, which is related to the photon lifetime τ_p, at frequency ω by $Q_T=\omega\tau_p$ is given by

$$\frac{1}{Q_T} = \frac{1}{Q_R} + \frac{1}{Q_i} \quad \text{..... (1)}$$

where $Q_R=\omega\tau_R$ and $Q_i=\omega\tau_i$, τ_R and τ_i represent the radiation loss and intrinsic cavity loss respectively. τ_R is given by:

$$\frac{1}{\tau_R} = \frac{P_R}{W_E} \quad \text{..... (2)}$$

where P_R denotes the total power radiated by the cavity and W_E denotes the stored energy in the cavity which is proportional to the cavity mode volume. Hence a method that reduces P_R and increases W_E will decrease the radiation loss from the cavity and hence increase the effective Q. A high Q implies that the light is trapped for a longer period of time in the cavity and hence interacts longer with any analyte in the vicinity of the photonic crystal microcavity. In addition, since W_E is proportional to the optical mode volume, a higher W_E leads to potential for larger optical mode overlap with the analyte which also contributes to higher sensitivity.

Our biosensor consists of a linear PC microcavity coupled to a PCW in a SOI platform. The PCW is a W1 line defect waveguide with uniform lattice constant *a*=400nm, where W1 denotes that width of the PCW is $\sqrt{3}a$. The third row of holes on either side of the PCW were shifted laterally in Γ–K direction by 0.1*a*. Silicon slab thickness and air hole diameter are *h*=0.58*a* and *d*=0.54*a*. In contrast to conventional devices which study L3 linear PC microcavities, with 3 missing holes along the Γ–K direction [17], or smaller hexagonal microcavities [5, 18] we study linear L13 PC microcavities with 13 missing holes along Γ–K direction. L13 PC microcavities are fabricated two periods away from the PCW. A scanning electron micrograph image of the L13 PC microcavity is shown in Fig. 2(a). The edge holes indicated by A and A', are shifted outward [19] in the Γ–K direction by 0.15*a*. While the L13 PC microcavity has several resonance modes, the resonance mode profile of interest is shown in Fig. 2(b). The lateral shift of the third row of holes leads to higher group index and thus higher coupling efficiencies at W1 PCW guided wavelengths farther away from the transmission band edge than the resonance mode studied here.

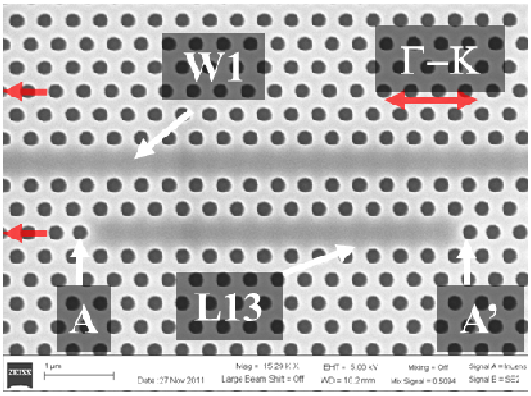

(a)

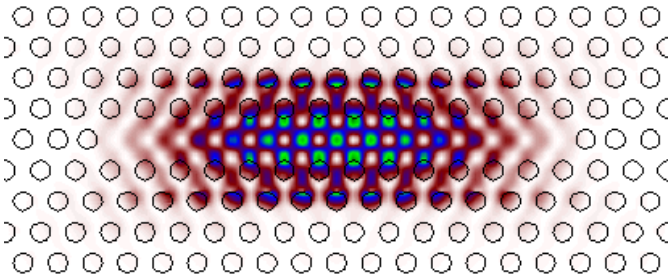

(b)

Fig. 2: (a) Scanning electron micrograph image of L13 PC microcavity coupled to W1 PC waveguide. The edge air holes are indicated by A and A' and the direction of shift indicated by the red arrows. (b) Resonance mode profile of L13 PC microcavity.

The higher Q in L13 PC microcavities is due to the combined effects of lower radiation loss as the resonance moves deeper into the photonic band gap compared to L3 PC microcavities [8, 16] that are studied conventionally, and the larger mode volume of L13 PC microcavities compared to L3 PC microcavities. Higher Q thus increases the ability to detect small changes in concentration. Furthermore, the slightly increased length enables larger overlap of the optical

mode with the analyte leading to higher sensitivity. We have shown [8, 16] that increasing the length of the PC microcavities to about 5.5μm in our L13 PC microcavities designed for operation at around 1550nm, from present targets of sub-μm, leads to higher Q and higher sensitivity in chemical sensing.

It must be noted here, that in the geometry selected here, the loss from the microcavity into the photonic crystal waveguide also contributes a term Q_{WG} to equation 1. Detailed analysis of the effect of Q_{WG} and further engineering to compensate for the effect of Q_{WG} are discussed elsewhere [20]. Q_{WG} is determined by the distance, in terms of number of periods, of the PC microcavity from the PCW as well as the orientation of the PC microcavity with respect to the PCW. Research in ref. [20] has determined that the optimum Q_{WG} balances the distance from the PCW and the coupling efficiency between the waveguide and the microcavity.

4. DEVICE FABRICATION

The device fabrication has been described in detail in Ref. [16]. Upon fabrication, wafers were functionalized by treating with 10% by volume 3-APTES in toluene. It is then washed 3 times in toluene to remove unbound 3-APTES, 3 times in methanol to remove toluene and finally 3 times in de-ionized water to remove methanol. The wafers are then incubated in 1% glutaraldehyde in phosphate buffered saline (PBS) for 5 minutes and washed 3 times in PBS and ink-jet printed with target antibodies in glycerol. Past research has shown that the 3-APTES-glutaraldehyde coupled layer retains its initial activity for several weeks [21]. Hence we do not expect any reduction in activity within the 30 minutes by which time the target antibodies are printed. The printed spots were left to incubate overnight. Subsequently, all target antibodies not bound to the functionalized device layer were removed by washing 3 times in PBS. After overnight incubation and washing, the device is coated with bovine serum albumin (BSA) to prevent any non-specific binding and washed 3 times with PBS. The device is now ready for measurements.

5. BIOSENSING RESULTS

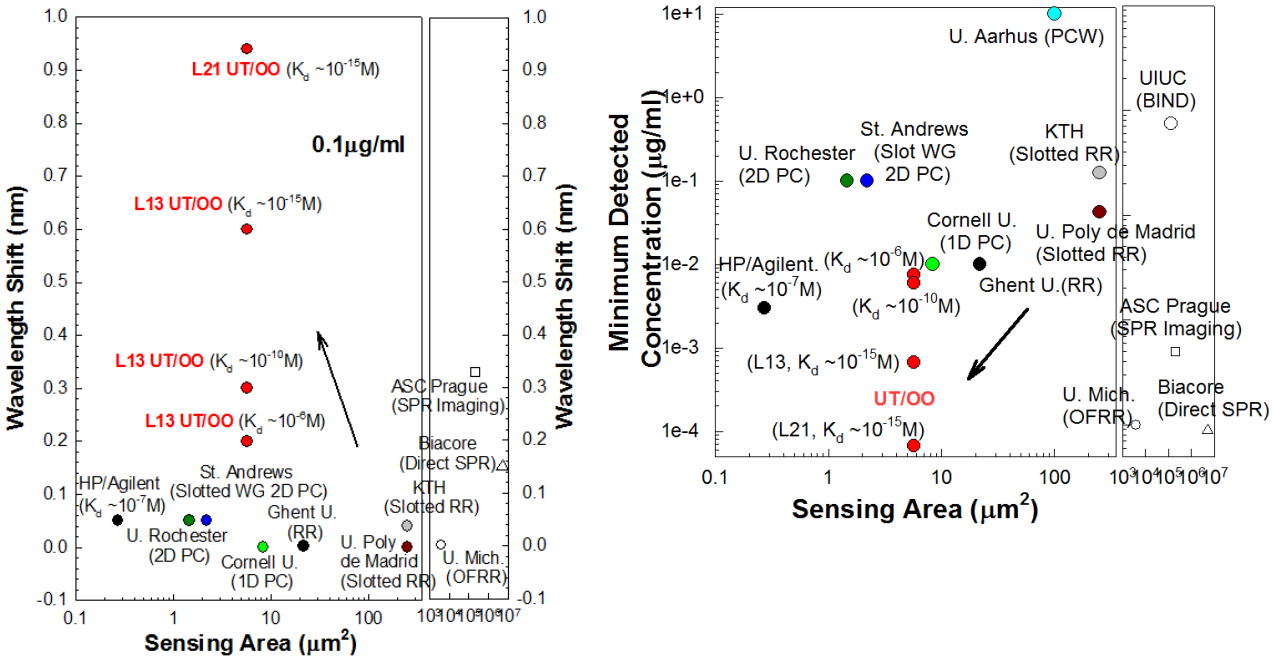

Fig. 3: (a) Comparison chart of PC based biosensors demonstrated here versus other label-free optical platforms as a function of sensing area on chip. Sensitivity comparison at mass concentration 100ng/ml. (b) Comparison of minimum detection limits of PC based biosensors demonstrated here versus other label-free optical platforms as a function of sensing area on chip. [13-14, 18, 24-28]

Details of biosensing have been covered elsewhere [16] and are not repeated here. In Fig. 3 we summarize the sensitivities and minimum experimentally detected concentrations of our photonic crystal platform and compare the results with other label-free platform studied in the literature. The sensitivity in Fig. 3(a) is measured as a function of the

resonance wavelength shift observed for different competing platforms at a concentration of 0.1μg/ml. The resonance wavelength shift observed in our platform is highest amongst all competing technologies. Recently, we have measured L21 and L55 PC microcavities (comprising 21 and 55 missing holes in the Γ−K direction along the length of the W1 PCW) coupled to W1 PCW. Fig. 3(b) shows that in L21 PC microcavities, the minimum experimentally detected concentration is 80 femtograms/mm^2 (calculated from the concentration of 1pM or 67pg/ml of binding of avidin to biotin). [20] The L55 PC microcavity detected a concentration of 50fM. Details of the design and measurement methods have been covered in a concurrent publication [22]. It is worthwhile to note that the length of a L21 PC microcavity is <10μm (length of L55 PC microcavity is ~22μm), 3 times smaller than the cavity length > 30μm of a ring resonator with diameter 10μm or nano-hole array based surface plasmon resonance devices (30μm×30μm)[23].

6. LUNG CANCER

Primary lung cancer develops from epithelial cells lining the airways of the lung. Normally, these epithelial cells form a crucial barrier between the internal and external environments and in the lung, these cells prevent leakage of blood while assisting with exchange of O2 and CO2. Exposure to airborne particles and toxins, especially those found in cigarette smoke, leads to genetic changes in epithelial cells which accumulate and underlie progressive changes from hyperplasia and dysplasia to carcinoma in situ and frank cancer. As such tumors grow, they outstrip supplies of blood and oxygen, become stressed, and undergo the epithelial-mesenchymal transition (EMT), a process by which cells switch their epithelial gene expression patterns to a mesenchymal phenotype with increased migratory and invasive properties. This process is thought to underlie metastatic potential in many tumor types. A facile method for detection of the EMT state of tumor samples would have major importance both clinically and for basic science investigations. We and others have shown that ZEB1 and ZEB2 have a prominent role in controlling the EMT process in lung cancer [29-30]. In this paper, we present proof-of-concept data that validate the ability of photonic crystal microcavity sensors to detect ZEB1 specifically via sandwich assays with high sensitivity.

We coupled the following antibodies or proteins to the PC resonance cavities; anti-MYC 9E10 (Sigma Aldrich, Cat #: A3833 MYC–tag 9E10), anti-ZEB1 (H102, Santa Cruz, Cat #: sc-25388), pre-immune mouse IgG (BD Pharmingen™, Mat. #: 557273), bovine serum albumin (Invitrogen, Cat #: 15561-020). Chemicals including 3-aminopropyl-triethoxy-silane (3-APTES) (Acros, CAS #:919-30-2) and glutaraldehyde (Fischer Scientific, CAS#111-30-8) were used to functionalize the silicon surface using published procedures [10, 20-21]. Devices were routinely washed 3 times in PBS before measurements and after each addition of target lysate.

The lung cancer cell line NCI- H358 was obtained from the Tissue Culture Core facility of the Univ. of Colorado Cancer Center, Aurora, CO. It was stably transfected with a tetracycline-inducible 6myc-ZEB1 expression construct, as described by [29].

7. MEASUREMENTS

A typical transmission spectrum of the W1 PCW device immersed in phosphate buffered saline (PBS) is shown in Fig. 4. The coupled L13 PC microcavity device was covered with a representative probe capture antibody. The experimentally confirmed Q-factor in SOI is approximately 13,000, obtained as $\lambda/\Delta\lambda$ from the inset. In a multiplexed design, four L13 PC microcavities are arrayed on the four arms of a multimode interference (MMI) power splitter for simultaneous detection, as shown in Fig. 5[11].

In H358-ZEB1 lung cancer cells, expression of the ZEB1 gene was controlled with the tetraycycline derivative, doxycycline. Exogenous ZEB1 (MW = ~180 kDa) was tagged at the N-terminus with 6 copies of the MYC epitope, permitting recognition by the anti-myc antibody, 9E10. Samples were prepared from these cells prior to induction (0-day lysate) or after 3 days dox treatment to induce 6myc-ZEB1 (3-day lysate). Exogenous 6myc-ZEB1 present in the induced lysates can be detected using either the 9E10 antibody or an antibody that binds to native ZEB1 (Fig. 6). This analysis verified that ZEB1 was strongly expressed in the dox-induced lysate (3d dox), was absent from the control lysate (0 dox), and that both antibodies are highly specific for ZEB1.

Surface functionalization is similar to that described in Sec. 4 and described in detail in ref. [31]. The measurement procedure is also described in detail in ref. [31] and is not repeated here.

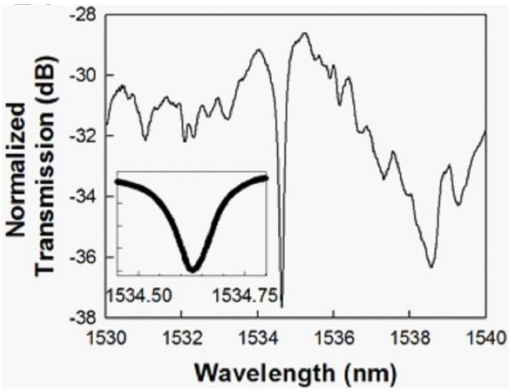

Fig. 4: Fiber-to-fiber normalized experimental output transmission spectrum of W1 PCW showing band edge at 1538nm and L13 PC microcavity resonance mode at 1534.5nm. (inset) magnifies the resonance frequency range.

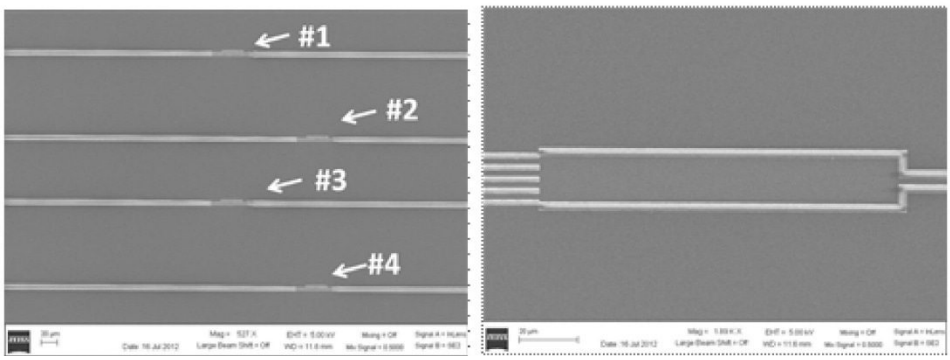

Fig. 5: Multiplexed device showing the 1×4MMI (right) and the photonic crystal sensor regions (left) on each arm. Arms are numbered.

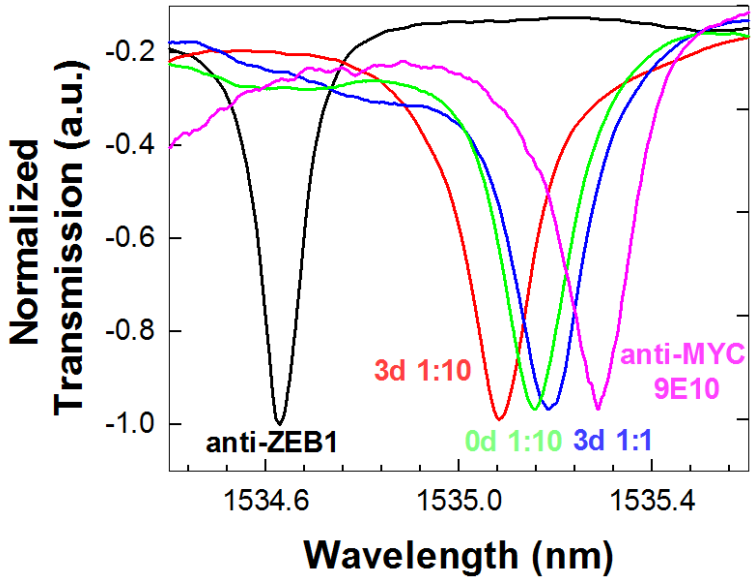

Fig. 6: Experimental transmission spectra as a function of added sample type/concentration. The respective sample legends are color coded according to the color of the experimental spectrum. The baseline transmission spectrum with probe capture anti-ZEB1 in PBS is indicated in black.

Fig. 6 plots the transmission spectra observed when 60µL of variously diluted 3-day induced lysates were added. A resonance wavelength shift from the anti-ZEB1 baseline (@ 1534.6 nm, black trace) was observed when the 3-day lysate (diluted 1:10 equivalent to 1000 cells per micro-liter) was added (red trace). A further shift was observed when 1:1 diluted 3-day lysate (equivalent to 5000 cells per micro-liter) was added (blue trace). Subsequent introduction of the 1:10 diluted 0-day lysate (which contains no detectable ZEB1) caused a small negative shift (green trace). This negative shift was within the range of wavelength accuracy of our optical spectrum analyzer and also the range of error observed from our control experiment. This result is consistent with the absence of any additional binding interaction from proteins in the 0-day induced lysate.

For confirmation that the resonance shift was specific for ZEB1 in the 3-day lysate, and not the result of non-specific interactions, a second antibody (anti-MYC 9E10, diluted 1:1000 in PBS) was introduced. The anti-MYC antibody was expected to bind the MYC-epitope tag attached to ZEB1 in the 3-day lysates. A secondary resonance wavelength shift was observed with anti-MYC, as shown by the pink trace in Fig. 7. The specificity of binding was thus confirmed by these sandwich assay measurements. The resonance wavelength shift observed over the entire sequence of sample additions for the BSA-coated control PC microcavity was within 0.02nm, which establishes the error margin of our device. Measurements with isotype-matched antibody further validated that the resonance super-shift resulted from 9E10 antibody binding to myc-tagged ZEB1 and was not confounded by non-specific background interactions [31].

In Fig. 7, the resonance wavelength shifts is plotted as a function of concentration or type of target sample solution. By switching the probe capture and secondary antibodies, a larger wavelength shift was observed in each case upon addition of the 3-day lysate (diluted in PBS to different concentrations), when the primary probe capture antibody bound to the silicon surface was anti-MYC 9E10 versus when the primary probe capture antibody was anti-ZEB1, as in Fig. 6. Similar higher sensitivities were observed in Western blot studies when anti-MYC 9E10 was used as the primary antibody instead of anti-ZEB1 (Fig. 8). We note that BSA failed to elicit detectable resonance shifts with any of the lysates tested, further supporting the specificity of the PC biosensor. The response of the biosensors is reproducible, the relative standard deviation (RSD) being 6.5% at the lysate concentration 3d 1:10 (1000 cells per micro-liter) for n=2 across different chips with 230nm silicon device layer in SOI.

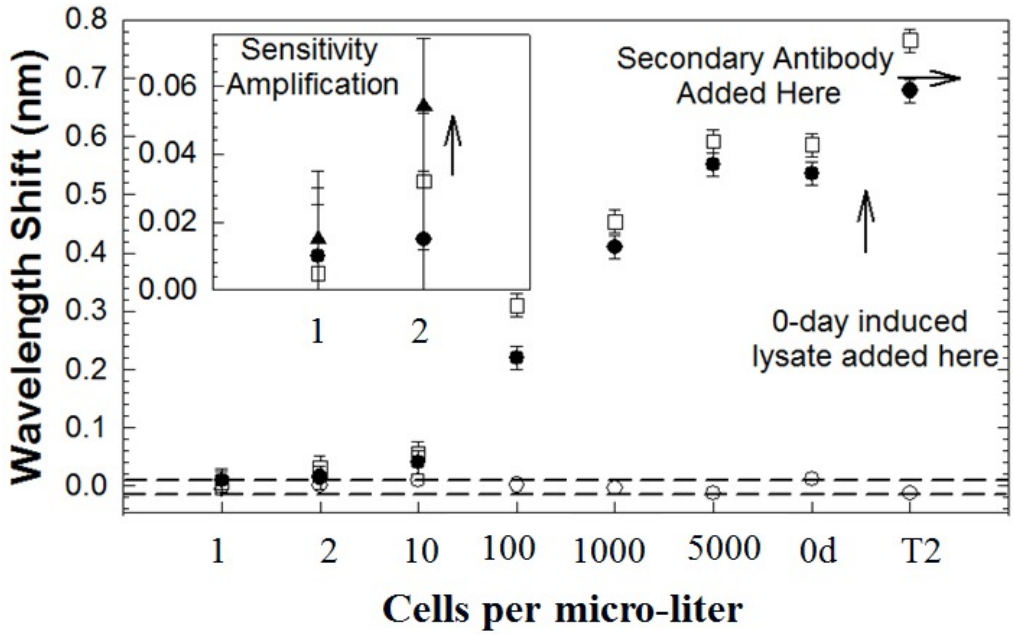

Fig. 7: L13 PC microcavity resonance wavelength shift as a function of concentration with anti-ZEB1 primary probe capture (filled circles) and anti-MYC 9E10 primary probe capture (open squares) antibodies. The secondary antibody T2 is anti-MYC 9E10 and anti-ZEB1 respectively for data plotted with filled circles and open squares. Control BSA coated L13 PC microcavity resonance as a function of position is plotted with open circles. (inset) Sandwich assay experiment at lowest concentration enables binding specificity verification and sensitivity amplification. Secondary anti-ZEB1 induced resonance shift indicated by filled triangles.

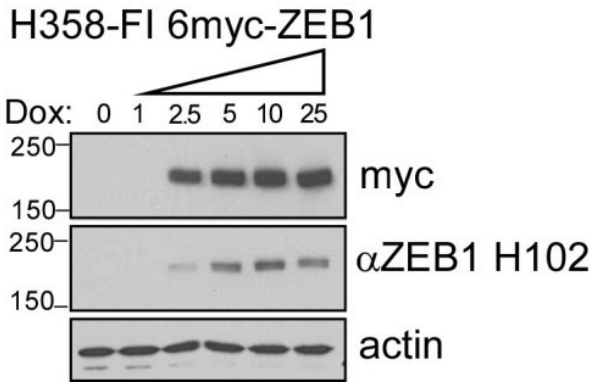

Fig. 8: Western blot analysis of doxycycline-induced 6-myc-ZEB1 expressed in NCI-H358 cells. Cultures were treated for 3 days prior to harvest with increasing doses of dox (ng/ml), as indicated. Protein lysates (10 μg/lane) were electrophoretically separated on 4-15% gradient SDS-PAGE gels and resulting blots were probed with 9E10 to detect the 6-myc tag and H102 to detect ZEB1 epitopes. Actin demonstrated equal loading.

The dashed lines indicate the wavelength shifts observed in the control experiment with BSA. Since no wavelength shifts should be theoretically observed in the control experiment, the boundaries indicated by the dashed lines represent the error margins in our measurement. The wavelength accuracy of the optical spectrum analyzer (Ando AQ6317B) of 0.02nm determines the measurement error margin for any resonance wavelength, as shown in Fig. 7. At the lowest concentration of 1:10,000 (1cell per micro-liter), the wavelength shift observed was less than 0.02nm, indicated by the dashed line in Fig. 8 and the device was considered unresponsive to this dilution.

The sandwich assay technique can amplify the resonance wavelength shift for small concentrations. Anti-ZEB1 and anti-MYC 9E10 antibodies recognize different epitopes of the induced ZEB1 in NCI-H358 cell lysates, but do not bind to each other. We functionalized a device using anti-MYC 9E10 as the capture antibody and added 1:5,000 diluted (2 cells per micro-liter) 3-day lysate. We observed a resonance wavelength shift of 0.032nm upon lysate binding to primary anti-MYC 9E10 antibody with an additional wavelength shift when the secondary anti-ZEB1 antibody was added. We observed an additional resonance wavelength shift of 0.022nm, amplified from 0.032nm, to a total shift of 0.055nm as shown in Fig. 5 inset. With the 3-day 1:10,000 dilution (1cell per micro-liter), the total resonance wavelength shift was 0.015nm which is within the range of wavelength error 0.02nm of our measurements.

The specificity and sensitivity demonstrated by separate binding interactions with specific antibodies and non-binding with control antibodies was next demonstrated simultaneously by multiplexing PC microcavities in a MMI power splitter. Details are provided in Ref. [31].

The PC device comprising the L13 PC microcavity coupled to the W1 PC waveguide, with the sandwich assay, thus demonstrated the capability to specifically detect ZEB1 in 2 cells per microliter of induced NCI-H358 cell lysates. Specificity was further established by multiplexing the binding and negative control antibodies, allowing simultaneous measurements of the same sample in the same instant of time.

8. DISCUSSIONS

The biomarkers that were used to demonstrate the sandwich assay technique in the proof-of-concept experiments in this paper, may be considered as a type of labeling, since we incorporated a MYC epitope which can be recognized by the anti-MYC antibody 9E10 in Western Blot tests. However, unlike sandwich ELISA methods, in which enzyme-linked antibodies are required to bind the detection antibody (secondary antibody as defined here) for signal generation, such requirement does not exist in our method. Users can simply design detection assays using a primary antibody and one to several second antibodies that recognize different specific epitopes of the target protein; in all cases, signal detection is performed by the photonic crystal. Such biomarkers are available and will be studied in the future for lung cancer detection [32-36]. Physical methods to further increase PC microcavity sensitivity are being investigated including optimization of PC microcavity length, the slow light effect in coupled PC waveguides and PC microcavity resonance mode quality factors [8, 10].

9. SUMMARY

To summarize, we demonstrated experimentally the specific detection of a relevant cancer-associated protein in lung cancer cell lysates with sensitivity down to 2 cells per micro-liter using PC microcavity biosensors in SOI devices. The combination of multiplexed resonance cavities with simultaneous detection permits duplicate or triplicate analyses in the same measurement for statistical confidence. Thus by combining multiplexing capability with sensitivity and specificity, our device provides a significant advantage over existing technologies for development of personalized diagnostic assays.

ACKNOWLEDGEMENTS

The authors acknowledge the National Cancer Institute for supporting this work under the Small Business Innovation Research (SBIR) program (Contract # HHSN261201000085C and HHSN261201200043C). RMG was supported by an NCI-sponsored SPORE CA58187. WCL, YZ and RTC also acknowledge support from AFOSR MURI (Contract # FA9550-08-1-0394).

REFERENCES

[1] Iqbal, M., Gleeson, M.A., Spaugh, B, Tybor, F., Gunn, W.G., Hochberg, M., Baehr-Jones, T., Bailey, R.C., and Gunn, L.C., "Label-Free Biosensor Arrays based on silicon ring resonators and high-speed optical scanning instrumentation," IEEE Journal of Selected Topics in Quantum Electronics 16(3), 654 (2010).
[2] Densmore, A., Vachon, M., Xu, D.X., Janz, S., Ma, R., Li, Y.H., Lopinski, G., Delage, A., Lapointe, J., Luebbert, C.C., Liu, Q.Y., Cheben, P., and Schmid, J.H., "Silicon photonic wire biosensor array for multiplexed real-time and label-free molecular detection," Optics Lett. 34, 3598-3600 (2009).
[3] Sipova, H., Zhang, S., Dudley, A.M., Galas, D., Wang, K., and Homola, J., "Surface plasmon resonance biosensor for rapid label-free detection of microribonucleic acid at subfemtomole level," Anal. Chem. 82, 10110-10115 (2010).
[4] Cunningham, B.T., Li, P., Schulz, S., Lin, B., Baird, C., Gerstenmaier, J., Genick, C., Wang, F., Fine, E., and Laing, L., "Label-free assays on the BIND system," J. Biomolecular Screening 9, 481 (2004).
[5] Lee, M., and Fauchet, P.M., "Two-dimensional silicon photonic crystal based biosensing platform for protein detection," Opt. Express 15, 4530-4535 (2007)
[6] Zlatanovic, S., Mirkarimi, L.W., Sigalas, M.M., Bynum, M.A., Chow, E., Robotti, K.M., Burr, G.W., Esener, S., and Grot, A., "Photonic crystal microcavity sensor for ultracompact monitoring of reaction kinetics and protein concentration," Sensors and Actuators B: Chemical 141 (1), 13 (2009).
[7] Lai, W-C., Chakravarty, S., Wang, X., Lin, C-Y., and Chen, R. T., "Photonic crystal slot waveguide absorption spectrometer for on-chip near-infrared spectroscopy of xylene in water," Appl. Phys. Lett. 98(2), 023304 (2011).
[8] Lai, W-C., Chakravarty, S., Zou, Y., and Chen, R.T., "Silicon nano-membrane based photonic crystal microcavities for high sensitivity bio-sensing," Optics Lett., 37(8), 1208-1210 (2012).
[9] Chow, E., Grot, A., Mirkarimi, L.W., Sigalas, M., and Girolami, G., "Ultracompact biochemical sensor built with two-dimensional photonic crystal microcavity," Optics Letters 29 (10), 1093 (2004).
[10] Chakravarty, S., Topoľančik, J., Bhattacharya, P., Chakrabarti, S., Kang, Y., and Meyerhoff, M.E., "Ion detection with photonic crystal microcavities," Opt. Lett. 30, 2578 (2005).
[11] Zou, Y., Chakravarty, S., Lai, W-C., Lin, C-Y., and Chen, R.T., "Methods to array photonic crystal microcavities for high throughput high sensitivity biosensing on a silicon-chip based platform," Lab Chip 12, 2309-2312 (2012).
[12] Voros,J., "The density and refractive index of adsorbing protein layers", Biophysical Journal 87 (1), 553 (2004).
[13] Skivesen, N., Tetu, A., Kristensen, M., Kjems, J., Frandsen, L.H., and Borel, P.I., "Photonic crystal waveguide biosensor," Optics Express 15 (6), 3169 (2007).
[14] Scullion, M.G., Di Falco, A., and Krauss, T. F., "Slotted photonic crystal cavities with integrated microfluidics for biosensing applications," Biosensors and Bioelectronics 27(1), 101-105 (2011).
[15] Tan, C.P., Cipriany, B. R., Lin, D. M., and Craighead, H. G., "Nanoscale resolution, multicomponent biomolecular arrays generated Tan, C. P. by aligned printing with parylene peel-off," Nano Lett, 10, 719-725 (2010).
[16] Chakravarty, S., Zou, Y., Lai, W-C., and Chen, R.T., "Slow light engineering for high Q high sensitivity photonic crystal microcavity biosensors in silicon," Biosensors and Bioelectronics 38(1), 170-176 (2012).

[17] Kang, C., Phare, C.T., Vlasov, Y.A., Assefa, S., and Weiss, S.M., "Photonic crystal slab sensor with enhanced surface area," Opt. Express 18(26), 27930 -27937(2010)
[18] Pal, S., Guillermain, E., Sriram, R., Miller, B.L., and Fauchet, P.M., "Silicon photonic crystal nanocavity-coupled waveguides for error-corrected optical biosensing," Biosensors and Bioelectronics 26, 4024-4031 (2011).
[19] Akahane, Y., Asano, T., Song, B.S., and Noda, S., "High-Q photonic nanocavity in a two-dimensional photonic crystal," Nature 425 (6961), 944 (2003).
[20] Zou, Y., Chakravarty, S., Kwong, D.N., Lai, W-C., Xu, X., Lin, X., Guo, Y., Hosseini, A., and Chen, R.T., "High yield high sensitivity silicon-based photonic crystal microcavity bio-sensors," (In Review)
[21] Subramanian, A., Kennel, S.J., Oden, P.I., Jacobson, K.B., Woodward, J., Doktycz, M.J., "Comparison of techniques for enzyme immobilization on silicon supports," Enzyme and Microbial Technology 24, 26-34, (1999).
[22] Zou, Y., Chakravarty, S., Lai, W-C., and Chen, R.T., "High yield silicon photonic crystal microcavity biosensors with 100fM detection limit," Paper 8570-9, SPIE Photonics West (2013).
[23] Chang, T-Y., Huang, M., Yanik, A. A., Tsai, H-Y., Shi, P., Aksu, S., Yanik, M. F., and Altug, H., "Large-Scale Plasmonic Microarrays for Label-Free High-Throughput Screening," Lab on a Chip, 11, 3596-3602 (2011).
[24] Dorfner, D., Zabel, T., Hürlimann, T., Hauke, N., Frandsen, L., Rant, U., Abstreiter, G., and Finley, J., "Photonic crystal nanostructures for optical biosensing applications," Biosensors and Bioelectronics, 24(12),3688–3692 (2009).
[25] Li, H., and Fan, X., "Characterization of sensing capability of optofluidic ring resonator biosensors," Applied Physics Letters 97,011105(2010).
[26] Barrios, C. A.,"Optical Slot-Waveguide Based Biochemical Sensors," Sensors 9,4751–4765, (2009).
[27] De Vos, K., Bartolozzi, I., Schacht, E., Bienstman, P., and Baets, R., "Silicon-on-insulator microring resonator for sensitive and label-free biosensing," Opt. Express 15(12), 7610–7615 (2007).
[28] Mandal, S., Erickson, D., "Nanoscale optofluidic sensor arrays," Optics Express 16(3), 1623–1631 (2008).
[29] Gemmill, R.M., Roche, J., Potiron, V.A., Nasarre, P., Mitas, M., Coldren, C.D., Helfrich, B.A., Garrrett-Mayer, E., Bunn, P.A., and Drabkin, H.A., "ZEB1-responsive genes in non-small cell lung cancer," Cancer Lett. 300 (1), 66-78 (2011).
[30] Takeyama, Y., Sato, M., Horio, M., Hase, T., Yoshida, K., Yokoyama, T., Nakashima, H., Hashimoto, N., Sekido, Y., Gazdar, A.F., Minna, J.D., Kondo, M., Hasegawa, Y., "Knockdown of ZEB1, a master epithelial-to-mesenchymal transition (EMT) gene, suppresses anchorage-independent cell growth of lung cancer cells," Cancer Lett. 296 (2), 216-224 (2010).
[31] Chakravarty, S., Lai, W-C., Zou, Y., Drabkin, H.A., Gemmill, R.M., Simon, G.R., Chin, S.H., and Chen, R.T., "Multiplexed specific label-free detection of NCI-H358 lung cancer cell line lysates with silicon based photonic crystal microcavity biosensors," Biosensors and Bioelectronics 43, 50-55 (2013).
[32] Takenaka, M., Hanagiri, T., Shinohara, S., Kuwata, T., Chikaishi, Y., Oka, S., Shigematsu, Y., Nagata, Y., Shimokawa, H., Nakagawa, M., Uramoto, H., So, T., Tanaka, F., "The Prognostic Significance of HER2 Overexpression in Non-small Cell Lung Cancer," Anticancer Res. 31, 4631-4636 (2012).
[33] Tretiakova, M., Salama, A.K., Karrison, T., Ferguson, M.K., Husain, A.N., Vokes, E.E., Salgia, R., "MET and Phosphorylated MET as Potential Biomarkers in Lung Cancer," J. Environ. Pathol. Toxicol. Oncol. 30, 341-354 (2011).
[34] Pesta, M., Kulda, V., Kucera, R., Pesek, M., Vrzalova, J., Liska, V., Pecen, L., Treska, V., Safranek, J., Prazakova, M., Vycital, O., Bruha, J., Holubec, L., Topolan, O., "Prognostic Significance of TIMP-1 in Non-small Cell Lung Cancer," Anticancer Res. 31 (11), 4031-4038 (2011).
[35] Tong, B.C., Harpole, D.H., Jr., "Molecular Markers for Incidence, Prognosis, and Response to Therapy," Surg. Oncol. Clin. N. Am. 21, 161-175 (2012).
[36] Ohira, T., Gemmill, R.M., Ferguson, K., Kusy, S., Roche, J., Brambilla, E., Zeng, C., Baron, A., Bemis, L., Erickson, P., Wilder, E., Rustgi, A., Kitajewski, J., Gabrielson, E., Bremnes, R., Franklin, W., Drabkin, H.A., "WNT7a induces E-cadherin in lung cancer cells," Proceedings of the National Academy of Sciences of the United States of America 100, 10429-10434 (2003).